Chemisorption of Organics on Platinum. 2. Chemisorption of C_2H_x and CH_x on Pt(111)

Jeremy Kua and William A. Goddard III*

Materials and Process Simulation Center, Beckman Institute (139-74), Division of Chemistry and Chemical Engineering, California Institute of Technology, Pasadena, California 91125

Received: June 8, 1998; In Final Form: August 18, 1998

Using the interstitial electron surface model (IESM) developed in the accompanying part, we examined the structures and energetics of a number of organic fragments on Pt surfaces. Using nonlocal density functional methods (B3LYP) we find that organics covalently bond to the Pt(111) surface with localized σ bonds to the surface Pt atoms, leading to tetrahedral hybridization of each carbon bonded to the surface. Thus, (i) CH_3 prefers an on-top site (a bond energy of ∼54 kcal/mol), (ii) CH_2 prefers a 2-fold bridge site (a bond energy of ∼104 kcal/mol), and (iii) CH prefers the fcc 3-fold bridge site (a bond energy of ∼167 kcal/mol). Similarly, C_2H_4 forms a strong (36 kcal/mol) di-σ bond (the π bond is BE = 8.5 kcal/mol), while $CHCH_2$ forms a tri-σ bond. The results for C_2H_x/Pt_8 are in good agreement with available experimental results on Pt(111) (π- and di-σ-bonded ethylene and ethylidyne). These results are used to obtain heats of formation (ΔH_f) for chemisorbed intermediates useful in estimating the energetics of various hydrocarbon intermediates on Pt surfaces. The application of these ΔH_f values is illustrated by considering ethylene hydrogenation and the decomposition of C_2H_4 on Pt(111).

1. Introduction

Supported platinum clusters catalyze a wide variety of hydrocarbon conversion reactions[1] involving C−C and C−H activation and are ubiquitous in the catalytic cracking and reforming processes used in the petrochemical industry. The chemistry of C_1 and C_2 hydrocarbons is fundamental to understanding this class of reactions. However, despite a great deal of progress on characterizing these systems,[2] there remain a number of uncertainities concerning the energetics, barriers, and mechanisms of even such simple reactions as hydrogenation/dehydrogenation.[3] The objective of this paper is to establish a framework useful for understanding the various reaction steps involved with hydrocarbon rearrangements on Pt surfaces. Subsequent studies will examine this and other reactions on other transition metal surfaces.

Previously (ref 4, referred to hereafter as part 1), we developed the interstitial electron model (IEM) for describing the bonding in platinum clusters. In that work, we concluded that the planar Pt_8 cluster in Figure 1 should serve as a good model for the structures and energies for hydrocarbons on Pt(111) surfaces.

Many important catalytic processes use highly dispersed Pt catalysts with clusters as small as 10 atoms. However, the best characterized systems involve studies on single crystal surfaces such as Pt(111). We will use clusters to examine both systems. The advantage of using clusters is that it allows one to zoom in directly on the details of a chemical reaction. For a bulk metal, the surface orbitals mix into bands, making it difficult to isolate which orbitals are essential to interactions with the adsorbate orbitals.

The strong interactions between nonmetal adsorbates and the metal surface generally split out a set of orbitals that can be regarded as localized in the vicinity of the adsorption site. We model this *localized vicinity* with a cluster chosen to have an effective configuration similar to the infinite surface. This enables us to focus directly on the interaction between orbitals of the metal surface and the adsorbate.

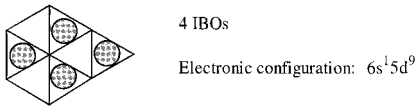

Figure 1. Pt_8 cluster model of the Pt(111) surface.

We have examined all C_1H_x and C_2H_x intermediates. This allows us to consider the hydrogenation and decomposition pathways of ethylene on Pt(111). These calculations on Pt_8 lead to geometries and energetics of ethylene (both π-bonding and di-σ-bonding modes) and ethylidyne, in good agreement with available experimental results.

2. Chemistry of CH_x on Pt(111)

2.1. Structures and Energetics. To establish the preferences of hydrocarbons for various sites on the Pt(111) surface, we calculated the optimum geometry of CH_3, CH_2, and CH in the top, bridge, and cap sites of Pt_8 (for the nonoptimal sites geometric constraints were applied). All calculations used the planar Pt_8 cluster fixed at the Pt−Pt bulk distance of 2.775 Å to represent the surface. The optimized structures are shown in Figure 2. Table 1 gives the binding energies and Pt−C bond distances of all these species. In each case, the preferred binding site is the one that allows carbon to make four σ bonds. Thus, the most stable structures are CH_3 in the on-top site (binding energy of 53.8 kcal/mol), CH_2 in the (2-fold) bridged site (binding energy of 104.3 = 2 × 52.2 kcal/mol), CH in the (3-fold) capped site (binding energy of 166.6 = 3 × 55.5 kcal/mol), and C in the (3-fold) capped site (binding energy of 153.57 = 3 × 51.2 kcal/mol). In addition, the total bond energy to the surface is proportional to the number of Pt−C bonds (53 ± 3 kcal/mol per bond). The C−Pt bond distances are 2.07 (CH_3), 2.01 (CH_2), 1.95 (CH), and 1.90 Å (C).

10.1021/jp982527s CCC: $15.00
Published on Web 11/03/1998

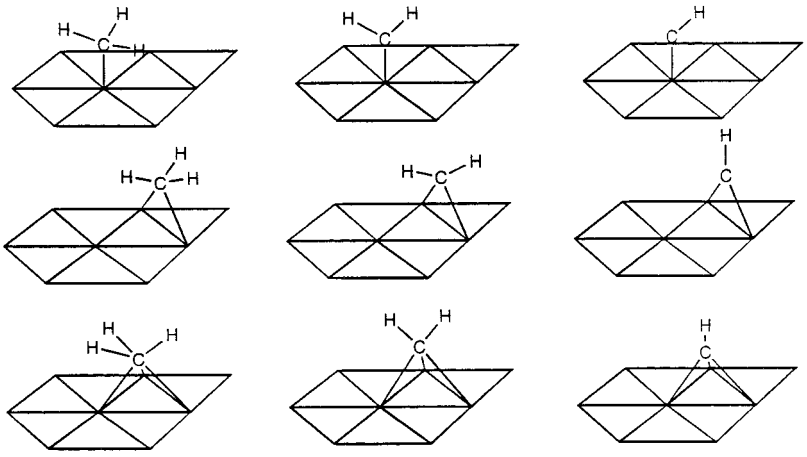

a. CH_x adsorbed at different sites

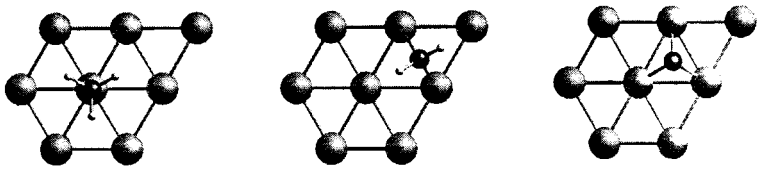

Pt_8-CH_3 (top site) Pt_8-CH_2 (bridge site) Pt_8-CH (cap site)

b. Top view of best binding structures of CH_x

Figure 2. CH_x adsorbed on Pt_8.

TABLE 1: Binding Energies and Pt−C Distances of CH_x/Pt_8 Clusters

site	CH_3	CH_2	CH	C
	Binding Energy (kcal/mol)			
top	53.77	78.07	80.93	
bridge	26.87	104.28	149.37	
cap	22.52	80.54	166.60	152.01
	Pt−C Bond Distances (Å)			
top	2.07	1.84	1.88	
bridge	2.41	2.01	1.86	
cap	2.63	2.11	1.95	1.90

Each adsorbate was allowed to optimize freely, and only the lowest energy (strongest binding) structures are reported. The spin state of the cluster chosen is the one lowest in energy (ground state). The calculated ground state of Pt_8 is $S = 3$, which is our reference state. The ground state for CH_3/Pt_8 is $S = 5/2$, which arises from spin pairing the dangling bond electron of CH_3 with an unpaired spin of Pt_8. The ground state of CH_2/Pt_8 is $S = 2$, which arises from spin pairing the two unpaired electrons of CH_2 with two unpaired spins of Pt_8. For CH/Pt_8, we find a net spin of $S = 5/2$. Since the ground state of CH is $S = 1/2$, this would be expected by spin pairing rules (the low-spin coupling of Pt_8 with $S = 3$ and CH with $S = 1/2$ would be $S = 5/2$).

Table 2a summarizes the spin states used and the calculated absolute energy and heats of formation for each of these species. Table 2b shows the optimized energies and ground spin states of the fragments.

2.2. Comparison with Experiment. There is kinetic and spectroscopic evidence for methyl, methylene (CH_2), and methylidyne (CH) moieties on Pt(111).[5] However, neither the energetics nor the structures for CH_x species adsorbed on Pt(111) have been sufficiently characterized experimentally to provide a test for calculations.

TABLE 2

a. Calculated Energies, Heats of Formation, and Spin States of C_2H_x/Pt_8 Clusters and H/Pt_8

adsorbate on Pt_8	site	S	absolute energy (hartrees)	heat of formation (kcal/mol)
CH_3 (+1H)	top	5/2	−993.184 32	−24.43
CH_2 (+2H)	bridge	2	−992.575 07	−23.27
CH (+3H)	cap	5/2	−992.002 22	−44.96
C (+4H)	cap	3	−991.344 25	−13.23
H	cap	5/2	−953.864 67	−11.38

b. Optimized CH_x Energies and Ground Spin States

fragment	S	absolute energy (hartrees)
CH_4	0	−40.524 05
CH_3	1/2	−39.841 37
CH_2	1	−39.151 63
CH	1/2	−38.479 47
C	1	−37.844 74

Low-energy electron irradiation of CH_4 on Pt(111) shows evidence of C−H bond cleavage to form chemisorbed methyl and chemisorbed hydrogen atoms.[6] Molecular beam surface scattering experiments find that the dissociative chemisorption of methane is enhanced by increasing both the translational energy of methane and the surface temperature.[7]

Generating methyl adsorbed on Pt(111) via gas-phase pyrolysis of azomethane allows the study of its chemistry by temperature-programmed desorption (TPD) and reflection−adsorption infrared spectroscopy (RAIRS).[8] The surface chemistry of methyl is characterized by a competition between hydrogenation (to produce methane) and dehydrogenation (which ultimately leads to the production of surface carbon). An early TPD and RAIRS study using methyl iodide as a precursor to form chemisorbed methyl on Pt(111) concluded, from deuterium exchange reactions, that the final hydrogenation step to form methane is preceded by multiple exchange reactions.

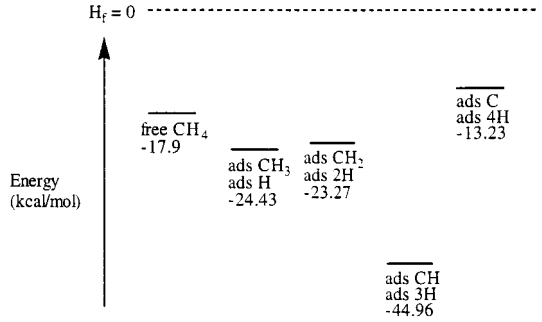

Figure 3. Heats of formation of CH_x species.

TABLE 3: Calculated Energies and Assigned Heats of Formation of Reference Compounds

reference	absolute energy (hartrees)	experimental heat of formation (kcal/mol)	corrections (h)
Pt_8	−953.255 01	0	$E(Pt_8) = -953.257\ 26$
H_2	−1.178 53	0	$E(H_2) = -1.178\ 54$
CH_2CH_2	−78.593 79	+12.5[a]	$E(C) = -38.128\ 32$
CH_4	−40.524 05	−17.9[a]	$E(C) = -38.138\ 45$

[a] Reference 10.

It has been suggested that CH_2/Pt is much more reactive than CH_3/Pt and undergoes reversible conversion to CH before finally fully hydrogenating to methane.[9]

Considering the various CH_x species adsorbed on a Pt_8 planar cluster, we find CH to be the thermodynamic sink. The binding energies for each of these species (still unavailable from experiment) are in Table 1.

2.3. Heats of Formation. To study the energetics of hydrogenation/dehydrogenation reactions involving the chemisorbed CH_x species, it is useful to obtain the heats of formation for each chemisorbed species.

We calculated the lowest energy structures of all intermediates bound to the Pt cluster. The calculated energetics for the various intermediates are shown in Figure 3. We then converted these energetics to heats of formation by using appropriate reference compounds.

To calculate heats of formation, we must choose an appropriate ensemble of reference compounds (one for each element). We have chosen the following as the reference compounds: (a) Pt_8 (since all our calculations use this cluster) in the $S = 3$ state, which is assigned $\Delta H_f(Pt_8) = 0$, (b) free gas-phase H_2, which is assigned $\Delta H_f(H_2) = 0$, and (c) free gas-phase methane, which is assigned $\Delta H_f(CH_4) = -17.9$ kcal/mol $= -0.028\ 52$ hartrees.

The calculated energies of the reference compounds are shown in Table 3. Heats of formation for ethylene and methane are taken from gas-phase experimental values.[10] The method used to calculate heats of formation is as follows: since $H_f(Pt_8)$ and $H_f(H_2)$ are both zero, the *reference energy* for a hydrogen, $E(H)$ will be −0.589 27 hartrees (half the calculated value for free H_2). The *reference energy* of carbon, $E(C)$ is derived from

$$C + 2H_2 \rightarrow CH_4$$

which leads to

$$E(CH_4) = -40.524\ 05 = -0.028\ 52 \text{ hartrees} + E(C) + 4E(H)$$

where $E(C)$ is −38.138 45 hartrees. The *reference energy* for Pt_8 is $E(Pt) = -953.257\ 26$ hartrees.

TABLE 4

a. Calculated Energies, Heats of Formation, and Spin States of C_2H_x/Pt_8 Clusters

adsorbate on Pt_8	site	S	absolute energy (hartrees)	ΔH (kcal/mol)
$\cdot CH_2CH_3$ (−1H)	top	5/2	−1032.498 39	−12.55
$\dot{C}H_2\dot{C}H_2$ (di-σ)	bridge	2	−1031.908 52	−23.56
$H_2C{=}CH_2$ (π)	top	3	−1031.864 58	+4.02
$\cdot CHCH_3$	bridge	2	−1031.891 64	−12.96
$(\cdot\dot{C}\cdot)CH_3$ (+1H)	cap	5/2	−1031.330 96	−42.28
$\cdot CH\dot{C}H_2$ (+1H)	cap	5/2	−1031.310 67	−29.55
$H\dot{C}{=}\dot{C}H$ (+2H)	cap	2	−1030.710 21	−33.91
$\cdot\dot{C}{=}CH_2$ (+2H)	cap	3	−1030.671 34	−9.52
$\cdot\dot{C}{=}\dot{C}H$ (+3H)	cap−top	5/2	−1030.009 67	+24.53
$\cdot\dot{C}{=}C{:}$ (+4H)	cap−top	2	−1029.366 72	+46.84

b. Optimized C_2H_x Energies and Ground Spin States

fragment	S	absolute energy (hartrees)
$\cdot CH_2CH_3$	1/2	−79.163 69
$CH_2{=}CH_2$	0	−78.593 80
$\cdot CHCH_3$	1	−78.480 01
$:\dot{C}CH_3$	1/2	−77.827 13
$(\cdot\dot{C}\cdot)CH_3$	3/2	−77.775 54
$\cdot CH{=}CH_2$	1/2	−77.904 86
$HC{\equiv}CH$	0	−77.329 60
$:C{=}CH_2$	0	−77.263 38
$\cdot C{\equiv}CH$	1/2	−76.604 00
$:C{=}C:$	0	−75.882 41
$\cdot C{\equiv}C\cdot$	1	−75.867 90

To calculate the heat of formation of C_xH_y/Pt_8 clusters, we used the formula

$$H_f(C_xH_y/Pt_8) = \{E(C_xH_y) - E(Pt_8) - xE(C) - yE(H)\} \times 627.5096$$

For example, the heat of formation of methyl is

$$H_f(CH_3/Pt_8) = \{-993.18432 + 953.25726 + 2(38.13845) + 3(0.58927)\} \times 627.5096 = -13.05 \text{ kcal/mol}$$

In comparing C_xH_y clusters with various numbers of H atoms, we assume low-coverage conditions in which excess H atoms go onto the Pt surface in locations well separated from the carbon-containing species. Thus, in examining rearranged structures starting with (CH_4), we consider the ΔH_f to be

$$\Delta H_f(CH_x/Pt_8) + (4 - x)\,\Delta H_f(H/Pt_8)$$

Thus, methyl ($x = 3$) has one hydrogen less than methane, leading to $(4 - x) = 1$. Therefore, we add one increment of $H_f(H/Pt_8)$ to account for the heat of formation for the chemisorbed H. From Table 4a, $H_f(H/Pt_8) = -11.38$ kcal/mol. Hence,

$$H_f(CH_3)_{ads} + H_{ads} - 13.05 - 11.38 = -24.43 \text{ kcal/mol}$$

The heats of formation shown in Tables 2a and 4a have all been calculated and corrected using this scheme.

Table 2a shows these values with the necessary corrections for adsorbed hydrogen. Table 2b shows the optimized energies and ground spin states of the fragments. The reference compounds chosen are Pt_8, H_2, and methane. The procedure used is similar for the C_2H_x compounds with the exception that $E(C)$ is −38.128 32, since ethylene is used as the reference hydrocarbon. From Figure 3, we see that CH is the thermodynamic sink. The dissociative chemisorption of methane to CH_3 and H is downhill by 6.5 kcal/mol. Breaking the second

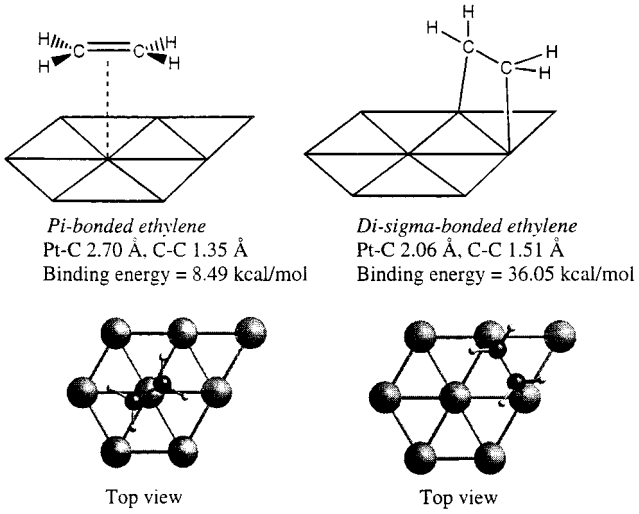

Figure 4. π- and di-σ-bonded ethylene on Pt_8.

C−H bond to form CH_2 adsorbed on the surface is only 1.2 kcal/mol uphill. Forming CH adsorbed is then downhill by 21.7 kcal/mol. The next step, currently being worked on, is to calculate activation barriers to determine a complete reaction profile for this series of reactions.

3. Ethylene Chemistry on Pt(111)

The chemistry of ethylene on Pt(111) has been studied extensively because it is a model reaction for understanding two major mechanisms in heterogeneous catalysis of hydrocarbon reactions: (1) hydrogenation to form ethane and (2) decomposition to finally deposit coke on the platinum surface. A barrage of experimental techniques have been used to study the mechanisms of these reactions, characterize the stable species, and identify the intermediates involved. However, only three species have been well-characterized: di-σ-bonded ethylene, π-bonded ethylene, and ethylidyne (CCH_3). The most stable species at low temperature is CCH_3. A consensus has not yet been reached for the mechanisms of catalytic hydrogenation and decomposition reactions.[3]

Recent studies using modern surface-sensitive techniques have made it possible to study and characterize a few of the C_2H_x species on Pt(111). The two important pieces of information are structural information (bond distances and angles) and adsorption or binding energy. Ethylene has been found to bind to the surface in two different modes, di-σ and π.

3.1. π-Bonded Ethylene. Ultraviolet photoemission spectroscopy (UPS) shows that ethylene adsorbs through its π-bonding orbital on clean Pt(111) below 52 K.[11] RAIRS concludes that the C═C bond is parallel to the surface and that the binding energy of this species is 9.6 ± 2.4 kcal/mol.[12] Our calculated structure of π-bonded ethylene at an on-top site on a Pt_8 planar cluster is in very good agreement with these results (see Figure 4). We calculate a binding energy of 8.49 kcal/mol and a C−C distance of 1.35 Å. The C═C bond is parallel to the surface, and the molecular plane is slightly tilted (92°). The Pt−C distances are calculated to be 2.70 Å.

3.2. Di-σ-Bonded Ethylene. The more stable mode of ethylene is the di-σ-bonding mode. When heated above 52 K, the π bond breaks and each carbon forms a single bond to a platinum atom. The C−C bond is parallel to and found above a Pt−Pt bridge. The molecular plane is tilted. This is suggested on the basis of high-resolution electron energy loss spectroscopy (HREELS),[13] UPS,[14] and NEXAFS[15] studies. The C−C bond measured from NEXAFS is 1.49 ± 0.04 Å. Initial TPD

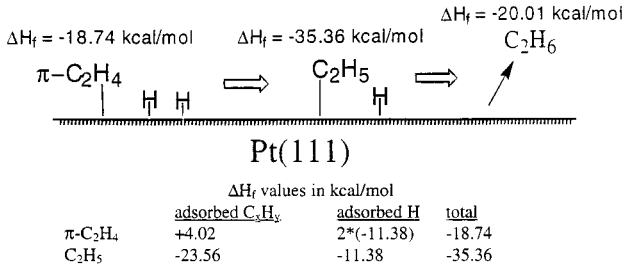

Figure 5. Horiuti−Polanyi mechanism for hydrogenation of ethylene.

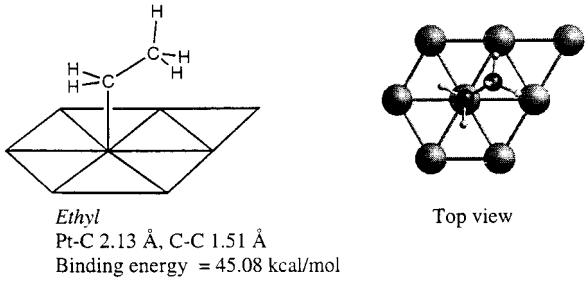

Figure 6. Ethyl (C_2H_5) on Pt_8.

experiments measured the adsorption energy to be 17 kcal/mol.[16] However, recent measurements by collision-induced desorption (CID)[17] suggest that this value is too small and that TPD does not accurately measure the binding energy of this species. Both CID and microcalorimetry[18] measure an adsorption energy ranging from 29.6 to 41.6 kcal/mol at low coverage. We calculate a binding energy of 36.05 kcal/mol and a C−C distance of 1.51 Å. The C−C bond is close to the bridged position and parallel to the surface and the tilt of the molecular plane is now much larger (115−116°). The Pt−C bond is 2.06 Å (see Figure 4).

3.3. Ethylene Hydrogenation. The hydrogenation reaction is thought to proceed via direct hydrogenation of ethylene to form an ethyl radical. Further hydrogenation of the ethyl radical leads to ethane desorbed from the platinum surface (see Figure 5). This mechanism was first proposed by Horiuti and Polanyi in the 1930s.[19] Recent evidence to support this mechanism comes from experiments using ultrahigh vacuum (UHV) techniques,[20] ^{14}C labeling studies,[21] and deuterium labeling experiments.[22] These studies conclude that the stable ethylidyne species is *not* an intermediate in the reaction but rather the hydrogenation incorporation occurs stepwise directly on the ethylene species. The ethyl radical is not a stable intermediate but readily undergoes β−H elimination to yield ethylene.[23] Structural and energetic information is not yet available on the transient ethyl species experimentally. Our calculations show that ethyl binds most stably at an on-top site with a binding energy of 48.60 kcal/mol (see Figure 6). The Pt−C distance is 2.13 Å, and the C−C bond length is 1.50 Å.

3.4. Ethylene Decomposition. The pathway for ethylene decomposition remains controversial. It is agreed that ethylidyne is the most stable of the C_2H_x species on Pt(111). Ethylene loses a net one hydrogen to form ethylidyne, which then eventually fully dehydrogenates at higher temperatures to deposit coke. Low-energy electron diffraction (LEED) studies show that ethylidyne occupies a 3-fold fcc site.[24] The C−C bond is perpendicular to the platinum surface, and the bond length is 1.50 ± 0.05 Å. The Pt−C bond length is measured to be 2.00 ± 0.05 Å. Our calculation of ethylidyne in the fcc site (see Figure 7) has the same geometry with an optimized C−C bond length of 1.49 Å. We further calculate a Pt−C bond length of 1.96 Å and a binding energy of 154.73 kcal/mol.

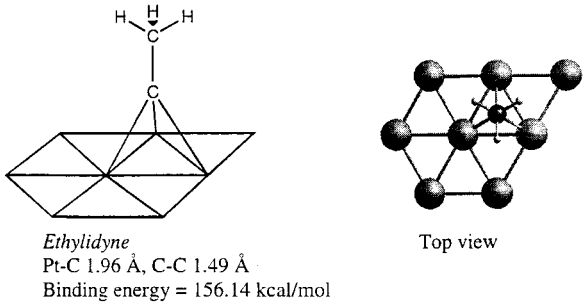

Figure 7. Ethylidyne (CCH_3) on Pt_8.

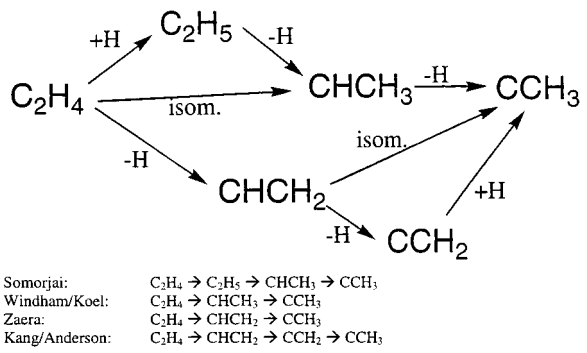

Figure 8. Four pathways for ethylene conversion to ethylidyne.

Four different pathways have been suggested for the conversion of ethylene to ethylidyne (see Figure 8). Two of these pathways (the middle two) are two-step reactions involving an isomerization step and a dehydrogenation step. They differ in which step comes first. The Windham−Koel pathway[16] proposes that ethylene first isomerizes to ethylidene ($CHCH_3$) and then undergoes α−H elimination to form ethylidyne. In the Zaera pathway,[22] dehydrogenation is the first step to form vinyl ($CHCH_2$), followed by isomerization to ethylidyne. The two other pathways that only have hydrogenation and dehydrogenation reactions are the Somorjai pathway,[25] which goes through the ethyl intermediate, and the Kang−Anderson pathway,[26] which includes vinylidene (CCH_2) as an intermediate. These latter two pathways are unlikely because ethyl readily undergoes β−H elimination and vinylidene transforms to ethylene at temperatures as low as 170 K.[3] It is suggested that ethylidyne undergoes successive dehydrogenation until coke is finally deposited on the platinum surface. At this point, no experiments clearly identify the intermediates in this reaction. Our calculations favor the Zaera pathway that goes through $CHCH_2$ as an intermediate.

3.5. Comparison to Previous Theory. Previous computational work on ethylene chemistry on Pt(111) has been limited to less accurate or semiempirical methods. Anderson and coworkers used extended Hückel theory with empirical two-body atom−atom corrections [the atom superposition electron delocalization molecular orbital (ASED-MO) method] in conjunction with a Pt_{15} planar cluster to calculate adsorption energies and reaction barriers.[27] The geometries show overly long bond distances for the adsorbed species. For example, the C−C bond lengths of adsorbed CCH_3, di-σ C_2H_4, and C_2H_5 were calculated to be 1.70, 1.77, and 1.73 Å, respectively (15−20% too large). The energetics also do not agree. ASED-MO leads to a binding energy of ∼90 kcal/mol for H to Pt(111), whereas the experimental value is ∼60 kcal/mol.

Another method of making predictions is to estimate the thermochemistry by calculating the heats of formation for the adsorbed species of all the intermediates involved.[28] This method involves (a) using electronic excitation energies, electron affinities, or ionization potentials to calculate a heat of formation for a gas-phase species that resembles the electronic state of an adsorbed molecule, (b) using measured heats of adsorption, and (c) using ab initio calculations to predict the heat of formation of adsorbed species. This method depends on the accuracy of the measured heats of formation of adsorbed species. Thus, some experimental numbers used in ref 28 are now thought to be incorrect. For example, the 17 kcal/mol TPD value[16] for the binding energy of ethylene was used, whereas recent experiments[17,18] suggest the correct value to be 30−42 kcal/mol.

3.6. Analysis of Energetics for C_2H_4 Conversion. Structures and binding energies of the strongest binding species for the other C_2H_x species are shown in Figure 9. From the heat of formation values for each of the clusters, with the appropriate corrections (Table 4a), we can consider the thermodynamics of all the C_2H_x species adsorbed on Pt(111). Figure 10 provides information to consider the pathways for ethylene conversion on Pt(111).

3.6.1. Hydrogenation. The heat of formation of ethane (not shown in Figure 10) is −20.0 kcal/mol.[10] For the first step of ethylene hydrogenation, thermodynamics favors the conversion of ethyl to ethylene. Although not calculated in these studies, we expect the barrier to this reaction to be small. Experimental evidence supports rapid β−H elimination.

Ethylidyne is the thermodynamic sink for the C_2H_x species in our calculations. This is in agreement with experimental evidence that ethylidyne does not participate as an intermediate in ethylene hydrogenation. Our calculations also suggest that the hydrogenation of π-bonded ethylene to ethyl is exothermic. Activation barriers need to be determined, but at this point, our calculations provide support for the Horiuti−Polanyi mechanism.

3.6.2. Decomposition. For the conversion of ethylene to ethylidyne, our energetics rule out the Kang−Anderson pathway. The conversion of $CHCH_2$ to CCH_2 is almost 20 kcal/mol uphill. It seems more likely that $CHCH_2$ isomerizes to form ethylidyne, according to the Zaera pathway. The Somorjai pathway is thermodynamically only slightly less favorable than the Windham−Koel pathway. However, the barrier to hydrogenation will need to be compared to the barrier to isomerization for a more complete comparison. When the two pathways that include an isomerization step are compared, the Zaera pathway seems to be more favorable, since $CHCH_2$ is 6 kcal/mol downhill from ethylene, while $CHCH_3$ is 10 kcal/mol uphill from ethylene.

3.7. Comparison of C_1H_x and C_2H_x. The C_2H_x compounds are closely related to the CH_x compounds on Pt(111). Interconversion between these two classes of compounds takes place via C−C bond breaking or C−C coupling reactions. Platinum metal is known to catalyze both these processes, of which isomerization of the carbon backbone in hydrocarbons is a good example. These reactions are expected to occur with higher activation energies compared to reactions that involve C−H bond forming and breaking. This is due to the directionality of the R_3C fragment orbital, which destabilizes the transition state where a metal−carbon bond is being converted to a C−C or C−H bond and vice versa. The spherical H 1s orbital can form multicenter bonds easily, and so the barrier for converting C−H bonds to metal−hydrogen bonds and vice versa is much lower than that for converting C−C bonds.[29]

Using Pt_8, H_2, and ethylene as reference compounds, we can examine the thermodynamics for the fragmentation reactions (see Figure 11). In general, the C_2H_x compounds on the right

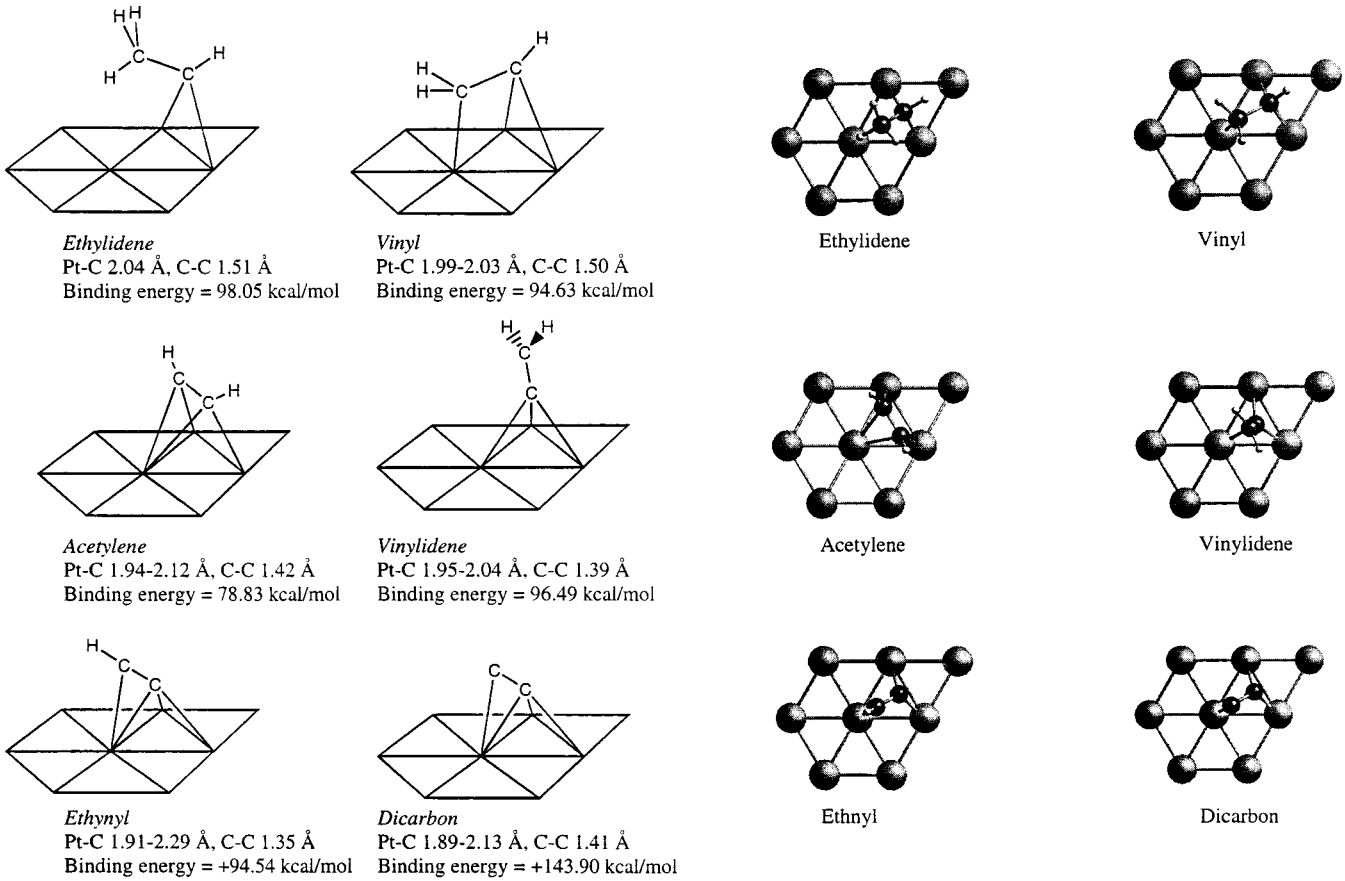

Figure 9. Intermediates in the ethylene decomposition reaction.

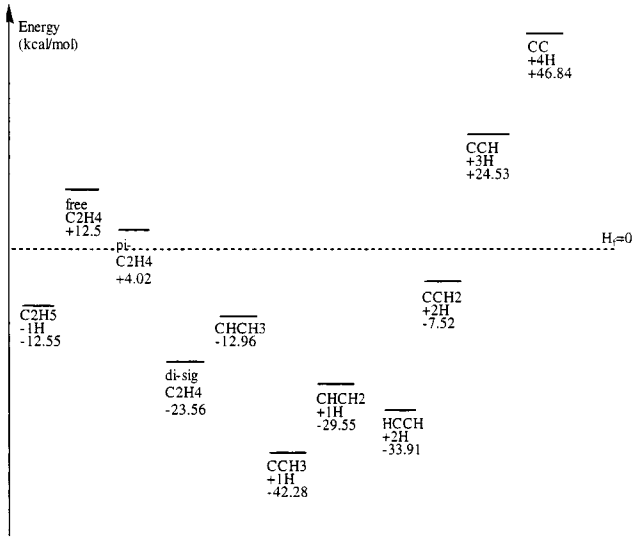

Figure 10. Heats of formation of C_2H_x species chemisorbed on Pt-(111).

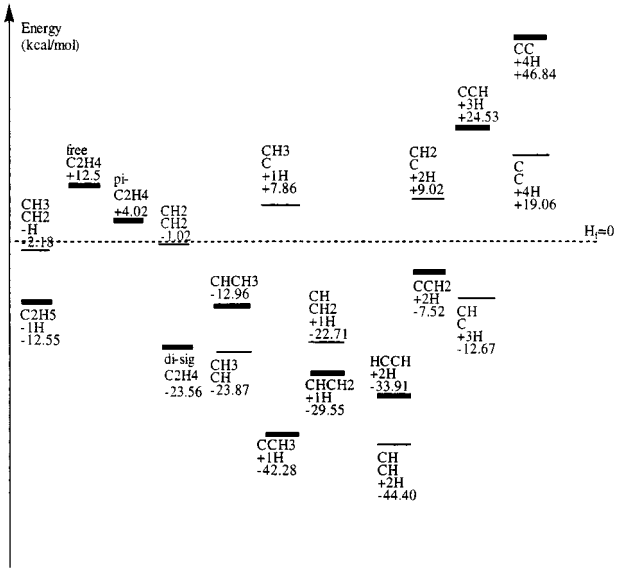

Figure 11. Heats of formation of C_2H_x and CH_y species.

side have fragments that are lower in energy, while compounds on the left side have higher energy fragments. This is largely due to the stability of the CH fragment. The thicker energy level lines correspond to the C_2H_x compounds (from Figure 10).

4. Hydrogen Chemisorption on Pt(111)

Extensive work has been done on the chemisorption of hydrogen on metals.[30] This is not surprising since hydrogenation and dehydrogenation reactions are among the most fundamental in industrial processes. The hydrogen molecule undergoes dissociative chemisorption on Pt(111) to form two separate chemisorbed hydrogen atoms. The development of HREELS has made it possible to study hydrogen adsorption on Pt(111). H is found to be most stable in the fcc site with a binding energy of 60 kcal/mol.[31]

In the computational area, periodic linearized augmented plane wave (LAPW) calculations of a H monolayer on Pt(111) has H in the fcc sites with a Pt−H bond length of 1.86 Å[32] for a bond energy of 61 kcal/mol. One-electron pseudopotential calculations[33] on Pt−H and Pt_2−H lead to binding energies that

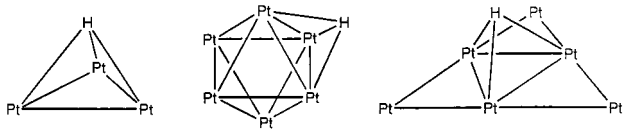

Figure 12. Optimized clusters of H adsorbed in the 3-fold sites of Pt_3 and Pt_6 clusters.

TABLE 5: Bond Distances (in Å) and Binding Energies (in kcal/mol) of H Capped in Pt_3 and Pt_6[a]

	H−Pt_3 (triangle)	H−Pt_6 (octahedron)	H−Pt_6 (triangle)
Pt−Pt	2.59	2.71 [9], 2.78 [3]	2.52 [6], 2.75 [3]
Pt−H	1.86	1.86	1.87
binding energy	59.04	59.64	56.06

[a] Number in brackets indicates number of bonds with same distance.

are too low (62 and 35 kcal/mol, respectively). Very extensive calculations have been done on Pt−H and Pt_2−H using high-level configuration interactions and spin−orbit coupling methods.[34] These lead to binding energies of 72 and 59 kcal/mol, respectively.

Our computational results on these same clusters using DFT NLDA-GGAII on Pt−H and Pt_2−H are in agreement with these results.

For the Pt−H molecule, we calculate an optimum Pt−H bond length of 1.52 Å and a binding energy of 68.77 kcal/mol.

For Pt_2−H, we find that H is bridge-bound with Pt−H lengths of 1.57 Å, a Pt−Pt length of 2.50 Å, and a binding energy of 58.80 kcal/mol.

Other studies on H binding to platinum clusters were concerned with studying the saturation of H on these clusters.[35,36] These do not directly utilize the cluster as a model for the platinum surface.

Our calculations of H in the capped site of different platinum clusters have Pt−H bond lengths of 1.86 Å and binding energies ranging from 56 to 60 kcal/mol, in good agreement with experimental results (60 kcal/mol). Full geometry optimized structures were calculated for Pt_3−H and Pt_6−H with H in the capped site. Pt_3 is a triangle, and for Pt_6, both the triangle and octahedron were calculated. The clusters are shown in Figure 12. Bond distances and binding energies are reported in Table 5. An IEM explanation for the binding of H to these small clusters has been explained in part 1.

Attempts to optimize H in the capped site of a Pt_4 tetrahedron were unsuccessful. H either moves to a bridged site or an η^1 site on the cluster. In the bridged site, the Pt−H bond length is 1.71 Å and the binding energy of H is 68.49 kcal/mol. The Pt−Pt bond lengths in this cluster range from 2.63 to 2.65 Å. The η^1-bound H has a Pt−H bond length of 1.56 Å and a binding energy of 70.97 kcal/mol. The higher binding energies are not surprising because these structures correspond to binding at defect (edge or corner) sites. It is also not surprising that the capped site of the tetrahedron is unstable for H adsorption, since the triangular faces of the tetrahedron represent hcp sites. Compare this to the octahedron where the faces represent fcc sites where H adsorbs with a binding energy of 56.6 kcal/mol. These results are well explained by the IEM (see part 1).

Constrained optimizations of H/Pt_8 were calculated using the B3LYP method (see Figure 13) since the C_xH_y/Pt_8 clusters were calculated using this hybrid method. The results are shown in Table 6. Once again, H in the cap site has the largest binding energy, in agreement with experiment. Hydrogens adsorbed in the top and bridged sites are only 0.5 and 1.8 kcal/mol less strongly bound. This suggests facile diffusion of H on the Pt-(111) surface.

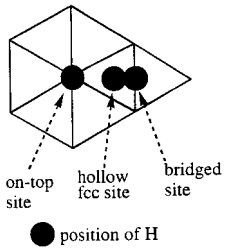

Figure 13. H adsorbed at different sites on Pt_8.

TABLE 6: B3LYP Constrained Optimizations of H/Pt_8

site	spin state	Pt−H (Å)	absolute energy (hartrees)	binding energy[a] (kcal/mol)
top	7/2	1.51	−953.863 81	66.69
bridge	2	1.74	−953.861 96	65.52
cap	5/2	1.86	−953.864 567	67.23

[a] Reference energies: Pt_8 ($S = 3$), −953.257 26 hartrees; H ($S = 1/2$), −0.500 27 hartrees.

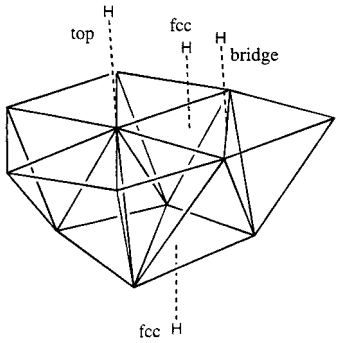

Figure 14. H adsorbed at different sites on Pt_{12} (8.4) bilayer cluster.

TABLE 7: B3LYP Constrained Optimizations of H/Pt_{12}[a]

site	spin (Å)	Pt−H (hartrees)	absolute energy (kcal/mol)	binding energy[b,c]
top (8-atom face)	9/2	1.55	−1430.665 46	64.90
bridge (8-atom face)	9/2	1.73	−1430.652 87	57.00
cap (8-atom face)	9/2	1.85	−1430.645 25	52.22
cap (4-atom face)	9/2	1.87	−1430.656 18	59.08

[a] In each case the spin is $S = 9/2$. [b] Reference energies: Pt_{12} ($S = 5$), −1430.061 76 hartrees; H ($S = 1/2$), −0.500 27 hartrees. [c] The excited states of the Pt_{12} (8.4) bilayer cluster are $S = 6$ at 5.13 kcal/mol and $S = 7$ at 11.84 kcal/mol.

We also did B3LYP constrained optimizations of H adsorbed on the Pt_{12} (8.4) bilayer cluster (shown in Figure 14). Note that this cluster does not have a s^1d^9 configuration. Pt−H bond lengths and binding energies are shown in Table 7. The ground spin state of the naked platinum cluster is $S = 5$. This is also the state predicted by IEM (four IBO in the four tetrahedra and an additional IBO associated with the fcc face of the octahedron on the four-atom face). The spin state used for the H/Pt_{12} clusters is therefore $S = 9/2$. There is now a larger discrimination in the energies of different sites on the eight-atom face. Bias for the on-top site is expected to be larger (from IEM) because of the fixed orientation of the tetrahedra with the tips pointing down. This is indeed the case from our calculations. More important is the comparison between the binding of H to the fcc sites on the eight-atom and four-atom faces. IEM predicts that the four-atom face fcc site has orbitals of mostly s character while the eight-atom face fcc site has orbitals of mostly d character. Hence, we expect stronger binding to the

TABLE 8: Binding Energy of Selected Pt_nCH_3 Clusters

cluster	S_{pred} from IEM of naked cluster	predicted electronic configuration	calcd binding energy (kcal/mol)
Pt atom		$s^1\,d^9$ (expt)	66.98
Pt_4 tetrahedron	1	$s^{0.5}\,d^{9.5}$	56.16
Pt_8 planar (C_{2v})	4	$s^1\,d^9$	53.77
Pt_{12} planar (C_{3v})	6	$s^1\,d^9$	52.23
Pt_7 hexagon	3	$s^{0.86}\,d^{9.14}$	43.47
Pt_{12} (8.4) bilayer	5	$s^{0.83}\,d^{9.17}$	41.39

four-atom face fcc site because of better overlap between the H 1s orbital and the s-character orbitals. From our calculations, the binding energy is lower at the eight-atom face fcc site (52.22 kcal/mol) compared to the 4-fold atom face fcc site (59.08 kcal/mol). The latter binding energy is also very close to the experimental binding energy of 60 kcal/mol.

5. Chemisorption of CH_3 on Selected Pt Clusters

It has been suggested that the use of naked metal clusters in calculating good chemisorption energies of adsorbates requires the cluster to be in a *prepared* bonding state.[37] The argument is that the excitations to higher states are involved in the *preparation*. For the infinite surface, this value is close to zero, but for a small cluster, the required excitation energy should be added to the calculated chemisorption energy of the ground state of the cluster. Using this rule, accurate chemisorption energies were calculated for H adsorbed to appropriate Ni clusters representing the Ni(111) and Ni(110) surfaces. More recently, this idea has been used to calculate the surface chemisorption of acetylene and ethylene to cluster models of the copper (100), (110), and (111) surfaces.[38] In di-σ-bonded ethylene, for example, there are two triplet states, a local triplet surface state and a triplet adsorbate state, which are coupled to produce a net singlet state for the two metal−carbon bonds. Chemisorbed ethylene, which is no longer planar, is akin to ethane in structure and bonding.

Our view is that one should choose the metal clusters so that the *ground state* has the same configuration as the semi-infinite metal surface. This should yield accurate chemisorption energies. The IEM suggests that Pt(111) has an s^1d^9 configuration and hence only clusters with this configuration are suitable.

To test this concept, we studied CH_3 chemisorption for several Pt clusters, as shown in Table 8. The Pt atom has an s^1d^9 configuration, but it has a significantly larger binding energy. This is not surprising, since unlike the other s^1d^9 clusters (and the extended surface), the atom has net two unpaired electrons rather than one. Pt_4 tetrahedron represents the smallest bilayer cluster that models binding to an on-top site. The binding energy is decreased significantly from that of the Pt atom. The other two s^1d^9 clusters, planar Pt_8 and Pt_{12}, have roughly similar binding energies. There is a slight decrease in binding energy from Pt_8 to Pt_{12}. The effect of adding more neighbors in different positions does not change binding significantly. Although the Pt_7 hexagon is very similar to planar Pt_8 (C_{2v}) in structure (the additional Pt atom not being connected to the central Pt that forms the Pt−C bond), the binding energies are 10 kcal/mol different. Indeed, the Pt_7 hexagon does *not* have the desired s^1d^9 configuration. The two layer Pt_{12} (8.4) has an electronic configuration close to Pt_7, leading to a binding energy in the same range. These results suggest that the electronic configuration of the cluster has a dominant effect on these calculations.

6. Conclusions

On the basis of the interstitial electron model, we chose a Pt_8 planar cluster to study adsorption and reaction pathways for chemisorption of C_1 and C_2 hydrocarbons on Pt(111). Using density functional methods with gradient corrections, we find geometries and energetics for C_2H_x clusters on Pt_8 in good agreement with experimental results (where available). The calculated energetics are in agreement with the Horiuti−Polanyi mechanism for hydrogenation to ethane. For the conversion of ethylene to ethylidyne, our results support the Zaera pathway (which goes through chemisorbed $CHCH_2$ as an intermediate). However, the Windham−Koel pathway (directly to $CHCH_3$ without going through $CHCH_2$) cannot be discounted. We have yet to determine the activation barriers.

These calculations show that for chemisorbed hydrocarbon fragments the most stable sites have four σ bonds to each fragment carbon. The calculated binding energies for H in the fcc site on small Pt clusters are in good agreement with experiment. On the planar cluster, the on-top site is slightly more favorable for H adsorption, a bias explained by the IEM.

These results suggest that relatively small clusters can be used to obtain accurate data for chemisorption *if* the clusters are properly chosen.

Appendix

Computational Methods. Calculations were carried out with nonlocal density functional theory (DFT) using two major methods. The first method is NLDA-GGAII, which uses the Slater local exchange functional[39] and the Perdew−Wang local correlation functional with the Perdew−Wang generalized gradient approximation (GGA-II) nonlocal correlation functionals.[40] This method is used for the study of the platinum clusters (see part 1) and hydrogen chemisorption on these clusters.

The second method is B3LYP, which uses the exact Hartree−Fock (HF) and Slater local exchange functional for the exchange terms using the Becke three-parameter method,[41] the Becke nonlocal gradient correction,[42] the Vosko−Wilk−Nusair exchange functional,[43] and the Lee−Yang−Parr local and nonlocal functional.[44] This method has been proven to be particularly good for calculating hydrocarbon species and is used in our calculations of CH_x and C_2H_x on platinum clusters.

All ab initio calculations were done using the PS-GVB (v2.35) and Jaguar programs.[45] The basis set used for platinum is the Hay and Wadt 18-electron relativistic effective-core potential.[46] For carbon and hydrogen, the 6-31G** basis set was used.

Acknowledgment. The research was funded by the NSF (CHE 95−22179). The facilities of the MSC are also supported by grants from DOE-ASCI, BP Chemical, Beckman Institute, Seiko-Epson, Exxon, Owens-Corning, Asahi Chemical, Chevron Petroleum Technology Co., Chevron Chemical Co., Chevron Research and Technology Corp., and Avery-Dennison. Some calculations were carried out at NCSA, University of Illinois.

References and Notes

(1) Davis, S. M.; Somorjai, G. A. *Hydrocarbon Conversion over Metal Catalysts* in *The Chemical Physics of Solid Surfaces and Heterogeneous Catalysis*; King, D. A., Woodruff, D. P., Eds.; Elsevier: New York, 1982; Vol. 4, p 217.

(2) Somorjai, G. A. *Chem. Rev.* **1996**, *96*, 1223.

(3) Zaera, F. *Langmuir* **1996**, *12*, 88.

(4) Kua, J.; Goddard, W. A., III Chemisorption of Organics on Platinum. Part I. The Interstitial Electron Model. *J. Phys. Chem.* **1998**, *102*, 9481.

(5) Zaera, F. *Langmuir* **1991**, *7*, 1998.

(6) Alberas-Sloan, D. J.; White, J. M. *Surf. Sci.* **1996**, *365*, 212.

(7) Valden, M.; Xiang, N.; Pere, J.; Pessa, M. *Appl. Surf. Sci.* **1996**, *99*, 83.
(8) Fairbrother, H. D.; Peng, X. D.; Trenary, M.; Stair, P. C. *J. Chem. Soc., Faraday Trans.* **1995**, *91*, 3619.
(9) Kemball, C. *Catal. Rev.* **1971**, *5*, 33.
(10) Chase, M. W., Jr.; Davies, C. A.; Downey, J. R., Jr.; Frurip, D. J.; McDonald, R. A.; Syverud, A. N. *J. Phys. Chem. Ref. Data* **1985**, *14* (Suppl, 1) 1.
(11) Cassuto, A.; Kiss, J.; White, J. M. *Surf. Sci.* **1991**, *255*, 289.
(12) Kubota, J.; Ichihara, S.; Kondo, J. N.; Domen, K.; Hirose, C. *Surf. Sci.* **1996**, *357/358*, 634.
(13) Steininger, H.; Ibach, H.; Lehwald, S. *Surf. Sci.* **1982**, *17*, 685.
(14) Felter, T. E.; Weinberg, W. H. *Surf. Sci.* **1981**, *103*, 265.
(15) Stohr, J.; Sette, F.; Johnson, A. L. *Phys. Rev. Lett.* **1984**, *53*, 1684.
(16) Windham, R. G.; Bartram, M. E.; Koel, B. E. *J. Phys. Chem.* **1988**, *92*, 2862.
(17) Szulczewski, G.; Levis, R. J. *J. Am. Chem. Soc.* **1996**, *118*, 3251.
(18) Yeo, Y. Y.; Stuck, A.; Wartnaby, C. E.; King, D. A. *Chem. Phys. Lett.* **1996**, *259*, 28.
(19) Horiuti, J.; Polany, M. *Trans. Faraday Soc.* **1934**, *30*, 1164.
(20) Cremer, P. S.; Su, X.; Shen, Y. R.; Somorjai, G. A. *J. Am. Chem. Soc.* **1996**, *118*, 2942.
(21) Davis, S. M.; Zaera, F.; Gordon, B.; Somorjai, G. A. *J. Catal.* **1985**, *92*, 250.
(22) Zaera, F. *J. Phys. Chem.* **1990**, *94*, 5090.
(23) Zaera, F. *J. Am. Chem. Soc.* **1989**, *111*, 8744.
(24) Starke, U.; Barbieri, A.; Materer, N.; Van Hove, M. A.; Somorjai, G. A. *Surf. Sci.* **1993**, *286*, 1.
(25) Somorjai, G. A.; Van Hove, M. A.; Bent, B. E. *J. Phys. Chem.* **1988**, *92*, 973.
(26) Kang, D. B.; Anderson, A. B. *Surf. Sci.* **1985**, *155*, 639.
(27) Anderson, A. B.; Choe, S. J. *J. Phys. Chem.* **1989**, *93*, 6145.
(28) Carter, E. A.; Koel, B. E. *Surf. Sci.* **1990**, *226*, 339.
(29) Low, J. J.; Goddard, W. A., III. *Organometallics* **1986**, *5*, 609.
(30) Christmann, K. *Surf. Sci. Rep.* **1988**, *9*, 1.
(31) Richter, L. J.; Ho, W. *Phys. Rev. B* **1987**, *36*, 9797.
(32) Feibelman, P. J.; Hamann, D. R. *Surf. Sci.* **1987**, *182*, 411.
(33) Zurita, S.; Rubio, J.; Illas, F.; Barthelate, J. C. *J. Chem. Phys.* **1996**, *104*, 8500.
(34) Balasubramaniam, K.; Feng, P. Y. *J. Chem. Phys.* **1990**, *92*, 541.
(35) Watari, N.; Ohnishi, S. *J. Chem. Phys.* **1997**, *106*, 7531.
(36) Minot, C.; Bigot, B.; Hariti, A. *J. Am. Chem. Soc.* **1986**, *108*, 196.
(37) Panas, I.; Schule, J.; Siegbahn, P.; Wahlgren, U. *Chem. Phys. Lett.* **1988**, *149*, 265.
(38) Triguero, L.; Pettersson, L. G. M.; Minaev, B.; Agren, H. *J. Chem. Phys.* **1998**, *108*, 1193.
(39) Slater, J. C. *Quantum Theory of Molecules and Solids*: *The Self-Consistent Field for Molecules and Solids*, McGraw-Hill: New York, 1974; Vol. 4.
(40) Perdew, J. P.; Chevary, J. A.; Vosko, S. H.; Jackson, K. A.; Pederson, M. R.; Singh, D. J.; Fiolhals, C. *Phys. Rev. B* **1992**, *46*, 6671.
(41) Becke, A. D. *J. Chem. Phys.* **1993**, *98*, 5648.
(42) Becke, A. D. *Phys. Rev. A* **1988**, *38*, 3098.
(43) Vosko, S. H.; Wilk, L.; Nusair, M. *Can. J. Phys.* **1980**, *58*, 1200.
(44) Lee, C.; Yang, W.; Parr, R. G. *Phys. Rev. B* **1988**, *37*, 785.
(45) *Jaguar 3.0*; Schrodinger, Inc.: Portland, OR, 1997. *PS-GVB*, version 2.3; Schrodinger, Inc.: Portland, OR, 1996.
(46) Hay, P. J.; Wadt, W. R. *J. Phys. Chem.* **1985**, *82*, 299.